Establishment of dopaminergic neuron purification system in mice for the Parkinson's disease study

Kit-Yeng Sheng
Osaka University
Hideki Hayakawa
Osaka University
Kousuke Baba
Osaka University
Yasuyoshi Kimura
Osaka University
Hideki Mochizuki
Osaka University
Toru Nakano
Osaka University
Shinpei Yamaguchi (yamaguchi@patho.med.osaka-u.ac.jp)
Osaka University

Research Article

Keywords: Parkinson's disease (PD), dopaminergic neuron purification

Posted Date: March 4th, 2021

DOI: https://doi.org/10.21203/rs.3.rs-296465/v1

Abstract

Parkinson's disease (PD) is a progressive neurodegenerative disorder characterized by the degeneration of dopaminergic (DA) neurons. The key neuropathological hallmarks in the brain of patients with PD are Lewy body (LB) inclusions, consisting of misfolded α-synuclein proteins. Despite extensive efforts, the molecular link between LB inclusions and DA neurodegeneration remains elusive because of the lack of a suitable approach. Here, we aimed to establish a novel dopa-decarboxylase (*Ddc*) fluorescent reporter mouse model that allows the identification and collection of DA neurons using a fluorescence-activated cell sorter. Successful enrichment of *Ddc*-expressing cells was validated by RNA-sequencing analysis. This approach allowed us to analyze the effect of α-synuclein accumulation on the DA neuron's transcriptome prior to neurodegeneration occurrence. We found that lipid-related process genes, followed by protein modification and degradation-related process genes, were upregulated in the α-synuclein-injected DA neurons. The activation of fatty acid-binding protein 1 (*Fabp1*) was particularly evident and confirmed by immunohistochemistry. Thus, our mouse model system and datasets provide a new method and insights into molecular mechanisms in PD.

Introduction

Dopaminergic (DA) neurons play a critical role in diverse functions, such as locomotion, learning, neuroendocrine control, reward, and motivation[1]. Degeneration or dysfunction of DA neurons results in mental, motor, and neurological disorders[1]. Particularly, Parkinson's disease (PD) is a progressive neurodegenerative disorder characterized by the loss of DA neurons in the substantia nigra pars compacta (SNc) of the midbrain[2–5]. Abnormalities in other types of neurons, such as serotonergic and cholinergic neurons, are also implicated during PD progression, resulting in non-motor symptoms[3,6]. Despite extensive studies, knowledge about the underlying cause of selective PD neurodegeneration remains lacking. The histopathological marker of PD is the presence of intraneuronal inclusions of Lewy bodies (LB), which mainly consist of accumulated misfolded α-synuclein protein[4,5]. Under physiological conditions, α-synuclein has been suggested to modulate neurotransmitter release and uptake through the assembly of the soluble N-ethylmaleimide-sensitive factor attachment protein receptor (SNARE) complex[4,7]. By contrast, the pathological α-synuclein adopts a beta-sheet conformation and aggregates into protofibrils[8,9]. It subsequently undergoes maturation by interacting with proteins, lipids, and organelles to form LB inclusions[9–12].

Increasing evidence has shown that the accumulation of α-synuclein impairs the biological function of DA neurons. For example, overexpression of α-synuclein downregulates the activity of VMAT2, a dopamine-transporting vesicular transporter, resulting in an accumulation of cytosolic dopamine metabolites and reactive oxygen species disrupting dopamine homeostasis[13]. Similarly, dopamine biosynthesis is affected by α-synuclein due to decreased tyrosine hydroxylase (Th) activity[14]. Further investigations revealed a presynaptic dopamine deficit increases DA neurons' vulnerability to oxidative stress[5,15,16]. Other mechanisms, such as activation of the neuroinflammation cascade induced by the

accumulated cytosolic reactive oxygen species and the LB formation process, have been proposed to cause DA neuron depletion[1,5,17,18]. However, the exact molecular mechanism(s) leading to neurodegeneration in PD is still elusive.

Despite the extensive efforts in establishing a suitable model for revealing the causal relationship of α-synuclein and DA neurodegeneration, neither the *in vivo* and the *in vitro* model was capable of reaching a clear conclusion. The available *in vivo* models, particularly the α-synuclein overexpressing transgenic mice and stereotaxic α-synuclein-injected mice, recapitulate the pathological signatures and symptoms of PD patients[19 – 22]. However, DA neurons are an anatomically heterogeneous cell population, and its purification is challenging because DA neurons form extensive and complex networks of synapses, which require harsh conditions for dissociation[23 – 26]. The collection of homogeneous neurons using a fluorescence-activated cell sorter (FACS) further induces stress in the neural cells. On the other hand, a homogenous DA neural population can be analyzed by the cell culture-based *in vitro* system[27,28]. But, DA neurons only survive for a short period of culture time that is not enough to observe the progressive neurodegeneration caused by the LB inclusions[27,28]. Furthermore, the interactions between DA neurons and the surrounding microenvironment are lacking in the *in vitro* model. This is likely one of the reasons it fails to reproduce cell death due to α-synuclein accumulation[27].

To address these problems, we established a novel knock-in mouse model bearing a humanized Kusabira-Orange 1 (hKO1) reporter cassette at the dopa-decarboxylase (*Ddc*, also known as *Aadc* or *Aaad*) gene locus (Ddc-hKO1) to facilitate the detection of DA neurons and developed an efficient purification method for the collection and downstream analyses. We applied this method in a PD model study and successfully investigated the gene expression changes in DA neurons caused by α-synuclein accumulation.

Results

Establishment of Ddc-hKO1 knock-in reporter mice

To visualize and purify DA neurons, we established a fluorescent reporter knock-in mouse targeting the *Ddc* gene. DDC is an enzyme responsible for the biosynthesis of dopamine and serotonin, and it is expressed in several types of neurons, including DA, serotonergic, cholinergic, and adrenergic neurons[29,30]. Using the CRISPR/Cas9-mediated homology-directed repair approach, we inserted a reporter cassette consisting of hKO1 conjugated with P2A self-cleaving peptide (Fig. 1a). After the transfection and clonal expansion of mouse embryonic stem cells (mESCs), successful knock-in was verified using PCR (Fig. 1b).

Ddc is highly expressed in DA neurons and embryonic cardiomyocytes[31]. Therefore, we examined whether the Ddc-hKO1 reporter recapitulated the endogenous expression of *Ddc* using *in vitro* differentiated cardiac cells from knock-in ESCs. Specific expression of hKO1 in spontaneous beating cells was confirmed at 20 days post-differentiation (Fig. 1c).

We then established a Ddc-hKO1 knock-in reporter mouse line through chimeric mouse generation using verified knock-in ESCs. No apparent abnormalities in embryonic development or growth were observed in the reporter mouse line (Fig. 1d). The adult mice were also healthy and fertile, producing a litter size similar to that of wild-type mice (data not shown).

hKO1 expression recapitulates the endogenous Ddc expression in reporter mouse brains

The hKO1 expression was observed in the left atrium and ventricle of the E15.5 embryonic heart, in addition to parts of the brain (Fig. 1e and Supplementary Fig. 1a). This expression pattern is consistent with the reported *Ddc* expression pattern and indicates the successful insertion of a reporter cassette to the *Ddc* locus[31].

Next, we evaluated the expression pattern of Ddc-hKO1 reporter in three developmental stages: prenatal (E15.5), neonatal (2 days after birth, P2), and adult (3 months old). At the prenatal stage, hKO1-positive cells resided in the midbrain and hindbrain regions (Fig. 2a and Supplementary Fig. 1a). Similarly, hKO1-positive cells were observed in the VTA and SNc in the midbrain and the dorsal raphe nucleus (DR) in the hindbrain of newborn pups and adult mice (Fig. 2b,c and Supplementary Fig. 1b,c). hKO1-positive cells were also detected in the arcuate nucleus (Arc) in the hypothalamus, retrorubral field (RRF), and locus coeruleus (LC) in the hindbrain of an adult mouse brain (Fig. 2c and Supplementary Fig. 1c). These expression patterns of hKO1 in the brain were completely in line with the reported *in situ* hybridization results of *Ddc* in the Allen Mouse Brain Atlas (www.brain-map.org)[32] and the Allen Developing Mouse Brain Atlas (http//developingmouse.brain-map.org). Additionally, no hKO1-positive cells were found in other brain regions, which is in good agreement with the reported *Ddc* expression pattern, and this is consistently observed in different generations of the reporter mice. These observations indicate that the reporter expression reflected the endogenous *Ddc* expression, and off-target insertion of the transgene cassette was less likely.

Figure 2 Expression pattern of Ddc-hKO1 in embryonic, neonatal, and adult mouse brains.(**a-c**) Representative images of vibratome sections of the whole brain in the coronal plane at E15.5 (**a**), P2 (**b**), and 3 months old (**c**). Thickness, 200 μm. Scale bar, 200 μm. MB, midbrain; HB, hindbrain; VTA, ventral tegmental area; SNc, substantia nigra pars compacta; DR, dorsal raphe nucleus; Arc, arcuate nucleus; RRF, retrorubral field; LC, locus coerules.</fig>

Purification of Ddc-expressing neurons using Ddc-hKO1 reporter mice

We used Ddc-hKO1 reporter mice to enrich *Ddc*-expressing neurons using FACS for subsequent downstream analyses such as RNA sequencing (RNA-seq). The regions containing hKO1-positive cells in adult mouse brains were micro-dissected and subjected to enzymatic digestion to obtain a single-cell suspension (Supplementary Fig. 2a). Pre-equilibration of media with 95% oxygen and supplementation of D-(+)-trehalose before and during the dissociation process are the two key factors that greatly enhance survivability of neurons[33]. *Ddc*-hKO1-positive cells were sorted based on the red fluorescence signals, and we successfully collected an average of 14,000 viable hKO1-positive neurons (approximately 1.5%) from

each brain (Fig. 3a, Supplementary Fig. 2b). We pooled two adult brains as one biological replicate for the following analyses to ensure sufficient yield and to minimize variation among samples.

Figure 3 Purification of dopaminergic neurons from Ddc-hKO1 mouse.(**a**) Representative FACS dot plots showing the gating strategy for the recovery of hKO1-positive neurons from Arc, VTA, SNc, DR, RRF, and LC of WT and Ddc-hKO1 mouse brains. Red dots represent the hKO1-positive neurons. (**b**) Scatter plot of RNA-Seq gene expression data comparing hKO1-positive and hKO1-negative populations. Fold change (FC) > 2. Red dots indicate genes highly expressed in hKO1-positive neurons, and blue dots indicate genes highly expressed in hKO1-negative neurons. (**c**) Heat map representation of expression levels of selected neuronal and non-neuronal marker genes. (**d**) Representative gene set enrichment analysis (GSEA) results enriched in hKO1-positive and hKO1-negative populations. VTA, ventral tegmental area; SNc, substantia nigra pars compacta; DR, dorsal raphe nucleus; Arc, arcuate nucleus; RRF, retrorubral field; LC, locus coerules; WT, wild type.</fig>

To verify that the purified hKO1-positive cells are viable *Ddc*-expressing neurons, we analyzed their transcriptome using RNA-sEq. Among the 24,346 mapped genes, 5,488 and 3,289 genes showed significantly higher expression in the hKO1-positive and hKO1-negative cells, respectively (fold change [FC] > 2, n = 2) (Fig. 3b). The marker genes for DA (*Ddc*, *Th*, *Slc6a3*, *Lmx1a*, *En1*), serotonergic (*Tph2*, *Slc6a4*, *Slc18a2*), and cholinergic neurons (*ChAT*, *Slc18a3*, *Ngf*) were highly expressed in the hKO1-positive population but not in the hKO1-negative population (Fig. 3c). By contrast, the marker genes for non-*Ddc*-expressing cells, such as GABAergic (*Slc6a11*, *Gabbr1*, *Slc6a1*), glutamatergic neurons (*Slc17a6*, *Slc17a7*, *Gls*), and astrocytes (*Slc1a2*, *Slc1a3*, *Gfap*), were highly expressed in the hKO1-negative population (Fig. 3c). Furthermore, we performed gene set enrichment analysis (GSEA) on all mapped genes to gain insights into the biological processes in both hKO1-positive and -negative populations. Biological processes, such as synaptic transmission in the DA neuron process (normalized enrichment score [NES] = 1.92), dopamine metabolic process (NES = 1.88), and dopamine transport (NES = 1.78), appeared on the top of the list of positively correlated enriched gene sets (Fig. 3d). In addition, gene sets related to catecholamine biosynthesis (NES = 1.95) and catecholamine metabolic processes (NES = 1.94) were also positively enriched. Meanwhile, biological processes, such as regulation of glutamate secretion (NES = -0.80), regulation of astrocyte differentiation (NES = -0.57), and negative regulation of the nervous system process (NES = -0.71), were negatively enriched (Fig. 3d). These results corroborate with the marker gene analysis demonstrating that the sorted hKO1-positive population indeed comprise *Ddc*-expressing neurons.

Among the selected pro-apoptotic markers, the expression of *Bad* and *Bax* was detected in both hKO1-positive and -negative populations (Supplementary Fig. 2c). Given that both *Bad* and *Bax* are expressed in the brain in the Allen Mouse Brain Atlas[32] and the BioGPS RNA-seq data (biogps.org)[34], the detected expression is likely due to basal level transcription. Notably, the expression of other apoptotic markers was either low or undetectable, and several anti-apoptotic marker genes, such as *Bcl2l1* and *Mcl1*, were highly expressed in both hKO1-positive and -negative populations (Supplementary Fig. 2c). Therefore, the

apoptosis pathway is suggested to be not activated during sorting. Taken together, we reasoned that our protocol is feasible for isolating viable *Ddc*-expressing neurons.

Gene expression profiling of the DA neurons during the early stage of α-synuclein accumulation

To investigate the gene expression changes in DA neurons caused by α-synuclein accumulation, we performed an intranigral injection of G51D α-synuclein into adult Ddc-hKO1 reporter mouse brains[19]. G51D α-synuclein is one of the mutations identified in familial PD, and the loss of DA neurons became detectable from 12 weeks onwards after the G51D α-synuclein (hereafter, α-synuclein) injection[19]. To analyze the effect of α-synuclein accumulation at an early stage, we collected DA neurons at 7 and 12 weeks post-injection prior to the onset of neurodegeneration (Fig. 4a)[19]. The assembly of α-synuclein and deposition of Lewy body-like inclusions in the VTA and SNc were confirmed by immunostaining (Fig. 4b). Consistent with a previous study, a loss of DA neurons was not observed at 7 weeks (Supplementary Fig. 3a,b).

Figure 4 Transcriptome profiling of α-synuclein accumulated neuron using Ddc-hKO1 mice.(**a**) Experimental scheme of transcriptome analysis of purified dopaminergic neurons from α-synuclein-injected brain. α-synuclein or saline was injected into the SNc of Ddc-hKO1 mouse brain unilaterally or bilaterally, and harvested at 7 weeks for immunohistochemistry and 7 or 12 weeks for RNA-seq analysis. (**b**) Representative images of immunohistochemistry of accumulated α-synuclein in the Ddc-hKO1 brain at 7 weeks. Scale bar, 100 μm. (**c**) Representative FACS dot plots showing the gating strategy for collecting survived hKO1-positive neurons from the injected brains. Red dots indicate hKO1-positive neurons. (**d**) Volcano plot showing the differentially expressed genes (DEGs) in hKO1-positive neurons between synuclein- and saline-injected mice. Upregulated and downregulated genes were highlighted by red and blue dots (FC > 1.5, FPKM > 1, $p < 0.05$) n = 3. (**e**) Heat map representation showing the classification of DEGs and gene numbers in each class. (**f**, **g**) Examples of DEGs in hKO1-positive neurons of α-synuclein-injected mice at 7 weeks (f) and 12 weeks (g). FACS, fluorescence-activated cell sorter; Sal, saline-injected; Syn, α-synuclein-injected brains. *P < 0.05, t-test, n = 3.</fig>

We proceeded with the collection of Ddc-hKO1-expressing cells from the VTA and SNc using the protocol established in this study (Supplementary Fig. 3c). The ratio and yield of hKO1-positive neurons harvested from saline-injected and α-synuclein-injected brains were comparable at both 7 and 12 weeks post-injection (n = 3, 2 brains per sample) (Fig. 4c, Supplementary Table 1, Supplementary Fig. 2d). This result supports a previous study showing that the loss of DA neurons was not evident as early as 12 weeks post-injection[19].

In total, 20,907 and 21,161 genes were commonly mapped by RNA-seq analysis in saline- and α-synuclein-injected samples at 7 and 12 weeks, respectively. The enrichment of viable DA neurons in the collected hKO1-positive population was confirmed using marker gene analysis (Supplementary Fig. 4a). DA neuron markers were highly expressed in all replicates with minimal expression of serotonergic neuron markers, suggesting that the major cell population collected from the VTA and SNc was of DA

neurons. The harvested neurons from saline- and α-synuclein-injected brains exhibited a similar expression pattern of apoptosis-related genes to untreated sorted hKO1-positive cells (Supplementary Fig. 3b,c). The small effects on apoptosis-related gene expression in both 7- and 12-week samples suggest that α-synuclein did not activate the apoptosis-related pathway. This result is also consistent with previous studies showing that neurodegeneration by α-synuclein accumulation is not mediated by apoptosis[2,13].

Early Biological Response During The α-synuclein Accumulation

We defined a set of genes in which its expression remained unchanged in the saline group at 7 and 12 weeks post-injection as a control to rule out the possible secondary effects (12,166 genes, FC < 1.5, P < 0.05). Differentially expressed genes (DEGs) were then determined by comparing expression changes between the α-synuclein and saline groups. Results showed 133 upregulated and 81 downregulated genes at 7 weeks post-injection, and 142 upregulated and 162 downregulated genes at 12 weeks post-injection (FC > 1.5, P < 0.05) (Fig. 4d). To analyze the functional enrichment of DEGs, we classified them into eight groups: upregulated at both 7 and 12 weeks (class 1, 4 genes), upregulated at 7 weeks but no change at 12 weeks (class 2, 60 genes), upregulated at 7 weeks but downregulated at 12 weeks (class 3, 1 gene), no change at 7 weeks but upregulated at 12 weeks (class 4, 117 genes), no change at 7 weeks but downregulated at 12 weeks (class 5, 122 genes), downregulated at both 7 weeks and 12 weeks (class 6, 2 genes), downregulated at 7 weeks but no change at 12 weeks (class 7, 47 genes), and downregulated at 7 weeks but upregulated at 12 weeks (class 8, 1 gene) (FC > 1.5, P < 0.05) (Fig. 4e). Among them, only classes 2 and 4 showed significant enrichment in specific biological terms. In class 2, a total of six biological processes were significantly enriched, and three of them were related to lipid metabolism processes, namely, lipid phosphorylation, glycerolipid metabolic process, and steroid metabolic processes, such as *Dgkb*, *Agk*, *Mvk*, and *Fabp1* (Fig. 4f, Supplementary Table 2). This result was supported by the GSEA result of gene expression profiles at 7 weeks without a pre-determined subset of genes (Supplementary Fig. 5). On the other hand, the gene set related to the protein-associated processes involved in the response to unfolded or misfolded proteins, including *Xbp1*, *Hdac8*, *Cry1*, and *Fbxo4*, was highly enriched in class 4 DEGs (Fig. 4g).

We focused on *Fabp1*, which is activated in the DA neurons at 7 weeks post-injection, because *Fabp3*, another fatty acid-binding protein family member, promotes oligomerization and uptake of α-synuclein in DA neurons[35,36]. We hypothesized that *Fabp1* may play a similar role as *Fabp3* in the early manifestation of PD progression. Immunohistochemical analysis demonstrated intense staining of FABP1 in DA neurons of the α-synuclein-injected brains (Fig. 5a). Furthermore, the number of FABP1-positive cells in the hKO1-positive neurons was also significantly increased (Fig. 5b). Therefore, we concluded that FABP1 expression in DA neurons was activated by α-synuclein accumulation.

Figure 5 FABP1 activation in the dopaminergic neurons during α-synuclein accumulation. (a) Representative immunostaining images showing the FABP1 expression in the VTA and SNc of injected mouse brains at 7 weeks. Scale bar: 100 μm. Dotted line indicates the VTA and SNc. **(b)** Bar graph showing the ratio of FABP1-positive cells in hKO1-positive cells at the VTA and SNc regions of saline- or

α-synuclein-injected mouse brains at 7 weeks. Each dot represents the actual value obtained from the individual mouse. FACS, fluorescence-activated cell sorter; VTA, ventral tegmental area; SNc, substantia nigra pars compacta; Sal, saline-injected; Syn, α-synuclein-injected. *P < 0.05, t-test, Sal: n = 3, Syn: n = 4. </fig>

Discussion

Elucidation of physiological function and profiling of DA neurons has remained challenging due to the difficulty in the manipulation and purification of homogenous neural population[25]. Currently, Th-green fluorescent protein (GFP) transgenic reporter mouse model is widely used to visualize living DA neurons[37,38]. This mouse line has a reporter cassette that is randomly integrated into the genome, and GFP expression is driven by a rat Th promoter. Although GFP expression is mainly observed in DA neurons, it is also detectable in non-DA neurons, potentially caused by the effects of the integration site of the transgene or a species-specific difference in the Th promoter[38]. The construction of the knock-in fluorescence reporter mice established in this study enable the visualization of *Ddc*-expressing cells and offer a great advantage in DA neurons' analysis. We developed an optimized protocol for efficient recovery of viable neurons by integrating two procedures: supplementation of D-(+)-trehalose and incubation with 95% oxygen. Both procedures significantly enhance the survivability of neurons during the enzymatic digestion of brain tissue[33]. We harvested more than 10,000 hKO1-positive cells from a single brain, which are sufficient for most downstream analyses such as RNA-seq, bisulfite sequencing, and ChIP-sequencing. Single-cell RNA-seq (scRNA-seq) has recently been used to obtain transcriptome profiling of small cell populations, including neurons[23,24,26,39]. Although scRNA-seq provides a great platform for profiling individual cells, technical issues such as high noise, low capture efficiency, and substantial cost remain. Our study utilizes a bulk RNA-seq approach using a reporter mouse, providing a reliable and robust protocol for the analysis of specific neuron types.

We utilized a PD model as a representative of nigrostriatal dopamine abnormalities. Although degeneration of DA neurons is the main hallmark of PD, its underlying molecular mechanism remained unclear[2,28]. This is mainly due to the lack of appropriate approaches. The *in vivo* α-synuclein injection model can recapitulate neurodegeneration, but it is impossible to harvest a homogeneous DA neuron population from wild type mice. On the other hand, *in vitro* culture experiments can enrich a homogeneous population, while it failed to reproduce cell death caused by α-synuclein[27]. Our reporter mouse model overcame these problems and succeeded in analyzing the transcriptome of α-synuclein accumulated DA neurons before and at the beginning of degeneration. Our results suggest apoptosis is not the cause of neurodegeneration as activation of apoptotic pathway genes was not detected in α-synuclein accumulated neurons. However, we cannot exclude the possibility of apoptosis at later stages because loss of DA neurons was not significant at 12 weeks post-injection. Further analysis at later stages using our reporter mice would allow us to unveil the pathways and molecular machinery of cell death in DA neurons.

Our transcriptome results demonstrated that the gene sets related to lipid-related processes, such as glycerolipid and lipid metabolic processes, were activated in DA neurons of the α-synuclein-injected brain at 7 weeks post-injection. Previous studies have shown that α-synuclein fibrils interact with lipids and other organelles during oligomerization to form Lewy body inclusions[9,10,12,40]. These gene sets include *Dgkb* and *Agk*, which are important for phosphorylation of diacylglycerol to phosphatidic acid, which play critical roles in intracellular signaling and phospholipid synthesis[41,42]. *Mvk* is involved in cholesterol and isoprenoid biosynthesis in the brain[43]. Given that 7 weeks is a short period of time since the α-synuclein injection, a large amount of lipid probably consumed for the on-going fibrilization of α-synuclein to form Lewy body-like inclusions. Additionally, the propagation of α-synuclein further attenuates the amount of lipids in DA neurons[12]. Thus, the lipid metabolic process may be upregulated to replenish the depleted pool of lipids in the cells. Our results suggest that abnormal lipid metabolism at the early stage of α-synuclein accumulation is one of the triggers of neurodegeneration.

On the other hand, most enriched gene sets of 12-week upregulated genes were involved in post-translational protein processes (Supplementary Table 2). For example, *Xbp1* is a key modulator of the unfolded protein response pathway associated with endoplasmic reticulum stress[44,45]. XBP1 has a neuroprotective function through the activation of endoplasmic reticulum chaperones, and the overexpression of XBP1 suppresses DA neurodegeneration caused by neurotoxin insult in overexpressing α-synuclein cell lines[44,45]. Another example is *Fbxo4*, an F-box protein; it is a component of the ubiquitin-protein isopeptide ligase SCF[46,47]. αβ-Crystallin, a binding partner of FBXO4, is a small heat shock protein that plays a role in preventing fibrillization of intracellular α-synuclein[46,47]. Therefore, activation of these genes may represent the proteolytic stress response of DA neurons induced by accumulated α-synuclein. Taken together, we propose that lipid metabolic processes followed by the unfolded protein response pathway are activated during the accumulation of α-synuclein in DA neurons.

We demonstrated that FABP1 was significantly upregulated in DA neurons of the α-synuclein-accumulated brain. *Fabp1* is a member of the fatty acid-binding protein family. A study using an *in vitro* system demonstrated that FABP3, another member of the same family, plays a role in promoting the oligomerization of α-synuclein in DA neurons[35,36]. FABP3 is a critical factor in the transportation of arachidonic acid, a polyunsaturated fatty acid[35]. FABP3 is also shown to directly bind to α-synuclein and promote oligomerization[35]. DA neurons lacking *Fabp3* were resistant to the neurotoxin agent MPP^+ insult. Therefore, *Fabp1* potentially plays a role similar to *Fabp3* in the oligomerization of α-synuclein at an early stage; however, this should be investigated further.

Apart from the PD model study, our reporter mice and neuron isolation protocol also offer other applications. For instance, it can be applied in the analysis of DA neuron subtypes, which show distinct expression patterns in marker genes[23,26,30,39]. Although scRNA-seq and immunohistochemical analyses demonstrate the heterogeneity of DA subpopulations in the brain, their specific function is still unclear. Different susceptibilities toward toxin treatment were previously observed among the subpopulations of DA neurons[26]. The dual reporter mouse systems, such as Ddc-hKO1/Th-GFP, would reveal the nature and

function of such subpopulations. Investigating the physiological function of these subpopulations may offer valuable insights into selective vulnerability in degeneration and drug development.

Additionally, the reporter mice are suitable for studying the effect of drug addiction and allelic expression dynamics of *Ddc* in the brain. *Ddc* was reported as an imprinting gene in the brain, where it shows controversial allelic expression patterns in different brain regions[48,49]. The advantage of Ddc-hKO1 reporter mice is the visualization of *Ddc* allelic expression in neurons. Heterozygous knock-in mice obtained from reciprocal crossing of Ddc-hKO1 and wild-type mice allow the analysis of allele-biased or mono-allelic expression of *Ddc* in a parent-of-origin manner. However, this study has some limitations. Since Ddc-hKO1 is expressed not only in DA neurons but also in other types of neurons, sophisticated microdissection is necessary to enrich DA neurons (Supplementary Fig. 3a). Also, the allelic expression of DA neurons at a single cell level may be challenging without the dual reporter mouse model that can visualize *Ddc* expression from both alleles with different fluorescence reporters.

In summary, the novel Ddc-hKO1 reporter mice not only offer an efficient purification system of neurons with high quality and quantity of yield, but are also a versatile mouse model applicable to investigate physiological changes in DA neurons and neural disorders, such as PD. To the best of our knowledge, this is the first transcriptomic dataset for DA neurons during the early accumulation of α-synuclein using a PD mouse model that mimics the symptoms of patients. We believe that our findings provide important insights into the molecular events that contribute to neurodegeneration which accelerates effective drug and therapies development.

Materials And Methods

Animals

All animal experiments were conducted with approval from the Animal Care and Use Committee of the Graduate School of Frontier Biosciences, Osaka University.
Mice were kept under standard laboratory conditions with controlled temperature and 12 h light/dark cycle with *ad libitum* access to food and water intake. All mice used in this study, including ICR and C57BL/6J, were purchased from Japan SLC (Hamamatsu, Japan). The day the vaginal plug was observed was defined as embryonic day 0.5 (E0.5).

Vector Construction For Ddc-hko1 Knock-in

Knock-in of the hKO1 cassette into the Ddc locus was conducted using CRISPR/Cas9-mediated homology-directed repair genome editing. The construction design of the Ddc-hKO1 donor vector is shown in Fig. 1a. The 5' homologous arm (HA), which is 732 bp upstream before the stop codon, and 3' HA, which is 602 bp downstream after the stop codon, were amplified from mouse genomic DNA using the following primer sets: 5' HA: forward, 5'-TCGAATTCGCGGATCCTTAGTCATTGGGAGTGGAG-3'; reverse, 5'-TAGTAGCTCCGGATCCTTCTTTCTCTGCCCTCAGC-3'; 3' HA: forward, 5'-ACGAAGTTATCTTAAGAGGCATCAGGATTCCAGC-3', reverse, 5'-

CGGTGGCGGCCTTAAGAGCTGGCAATGTAGCTCAG-3'. The single guide RNA target sequence of the insertion site was 5'-CAGGTAAGCTAGCTGCACCA-3'.

Cell Culture And Transfection

A G4 mouse embryonic stem cell line was used in this study[50]. ESCs were maintained under serum-free conditions (0.5× N-2 [Thermo Fisher Scientific, MA, USA], 0.5× B-27 [Thermo Fisher Scientific, MA, USA], 100 U/mL mouse LIF [Merck, NJ, USA], 3 μM CHIR99021 [Funakoshi, Tokyo, Japan], 1 μM PD0325901 [Stemgent, MA, USA], 1 mM L-glutamine [Nacalai Tesque, Kyoto, Japan], and 1× penicillin/streptomycin [Invitrogen, MA, USA] in DMEM/F-12 with GlutaMAX [Thermo Fisher Scientific, MA, USA]) in the absence of feeder layers. The donor vector and pX330 Cas9/single guide RNA vector were transfected into ESCs using Lipofectamine 2000 (Thermo Fisher Scientific, MA, USA). Successful knock-in of the reporter cassette was confirmed by PCR amplification. Primer sets for 5' and 3' insertion sites were as follows: forward, 5'-TGAAGCCTGAAACCAGCCCC-3', reverse, 5'-GCTCGAAGCAGTTGCCCCTCA-3'; and forward, 5'-ACGGCAGTTGGGATTCGTGA-3', reverse, 5'-CATGATGACCAAGTGTCTGAAAGGG-3', respectively.

Cardiac Lineage Differentiation Of Escs

Cardiac cell differentiation using Ddc-hKO1 ESCs was performed as previously described[51]. Briefly, ESCs were treated with 2.5 ng/mL of BMP-2 (Bio-Techne, Minnesota, USA) in propagation medium (100 mM non-essential amino acids [Thermo Fisher Scientific, MA, USA], 100 U/mL mouse LIF, 20 μM β-mercaptoethanol [Nacalai Tesque, Kyoto, Japan], 1× penicillin/streptomycin [Invitrogen, MA, USA], and 10% FBS [Nichirei, Tokyo, Japan] in DMEM/F-12 with GlutaMAX) for 24 h. ESCs were then passaged for embryoid body formation using the hanging drop method for 3 days. Embryoid bodies were collected in differentiation medium (100 mM non-essential amino acids, 20 μM β-mercaptoethanol, 1× penicillin/streptomycin (Invitrogen, MA, USA), and 20% FBS in DMEM/F-12 with GlutaMAX) and transferred to an ultra-low adhesion plate (Wako, Osaka, Japan) for 3 days to allow further differentiation under floating culture conditions. Embryoid bodies were plated on a cell culture dish coated with 0.1% gelatin (Sigma-Aldrich, Missouri, USA), and spontaneous beating cells were observed at approximately seven days after attachment.

Establishment Of Reporter Mice

Ddc-hKO1 chimeric mice were generated using the aggregation method. Briefly, 8-16-cell stage embryos were collected from the oviduct ampulla and uterus by flushing with M2 medium (Sigma-Aldrich, Missouri, USA) at E2.5. Zona pellucida was digested using 0.5% pronase (Sigma-Aldrich, Missouri, USA), and each morula was aggregated with Ddc-hKO1 ESCs. Following overnight incubation, chimeric blastocysts were transferred into the uterine of pseudo-pregnant ICR female mice. Chimeric mice were crossed with C57BL/6 female mice for several generations to maintain their C57BL/6J background. The primer sets for genotyping were as follows: forward, 5'-GTTTGTGCTACGCTTTGCTG-3'; reverse, 5'-CCTCAGGGTCATCTCCTGGT-3'.

Vibratome Sectioning And Imaging

Brains were collected from Ddc-hKO1 homozygous mice and fixed in 4% paraformaldehyde in phosphate buffered saline (4% PFA/PBS) overnight at 4°C. Fixed brains were embedded in freshly prepared 3% low-melting temperature agar before sectioning. Embedded brains were sectioned using a vibratome (Leica VT1000s; Leica Microsystems, Wetzlar, Germany) with a thickness of 200 μm and placed in chilled PBS. Sections were treated with 0.5× CUBIC-1, an animal tissue clearing reagent, for 24h, followed by 1× CUBIC-1 for another 24h[52]. Sections were mounted in 1× CUBIC-1 and imaged using a fluorescence microscope (BZ-X700; Keyence, Osaka, Japan).

Brain Dissociation And Cell Sorting Using A Facs

The brain dissociation protocol was performed with modification as previously described[53,54]. Homozygous knock-in Ddc-hKO1 mouse brains were harvested and placed in chilled 95% oxygenated hibernate A solution (Thermo Fisher Scientific, MA, USA). The VTA and SNc of the midbrain were micro-dissected in chilled dissection medium (20 mM HEPES [Nacalai Tesque, Kyoto, Japan], 10% [w/v] D-(+)-trehalose dihydrate [Nacalai Tesque, Kyoto, Japan] in HBSS (+) with phenol red [Nacalai Tesque, Kyoto, Japan]) saturated with 95% oxygen. The recovered VTA and SNc were minced into smaller blocks covered with dissection medium and immediately transferred into pre-warmed dissociation medium (10 U papain [Worthington, Ohio, USA], 2 mg DNase I [Sigma-Aldrich, Missouri, USA], and 4 U Dispase II [Sigma-Aldrich, Missouri, USA] in HBSS (+) with phenol red). After a 30-min incubation at 37 ºC, tissues were gently dissociated using a fire-polished glass pipette (approximately 40 μm of internal diameter). Brain suspension was resuspended with solution A (20 mM HEPES, 40 mg/mL BSA [Nacalai Tesque, Kyoto, Japan], 10% [w/v] D-(+)-trehalose dihydrate, 4 μL of RNase inhibitor [Nacalai Tesque, Kyoto, Japan] in HBSS without phenol red), followed by filtration using a cell strainer (pore size 40 μm). The filtrate was subjected to centrifugation, and the collected pellet was resuspended in solution B (0.9 M sucrose [Nacalai Tesque, Kyoto, Japan], 10% (w/v) D-(+)-trehalose dihydrate, 4 μL of RNase inhibitor in HBSS without phenol red, pH 7.5). Neuronal cells were concentrated by centrifugation in solution B. Finally, the cell pellet was washed again with solution A and resuspended in sorting medium (2% FBS [Thermo Fisher Scientific, MA, USA], 10% [w/v] D-(+)-trehalose dihydrate, 40 U RNase inhibitor [Thermo Fisher Scientific, MA, USA] in DMEM/F-12 without phenol red [Thermo Fisher Scientific, MA, USA]). All procedures were conducted on ice except for the digestion process. The hKO1-positive and -negative cells were sorted using a FACS (BD FACSAria III, BD Bioscience, USA) with 100 μm flow cells at a flow rate of 1.

RNA Purification And RNA-seq Analysis

hKO1-positive and -negative cells were collected by sorting into TRIzol LS reagent (Thermo Fisher Scientific, MA, USA). Cells from the two brains were pooled as one biological replicate. RNA purification was performed using a Direct-zol RNA microprep kit (Zymo Research, CA, USA) according to the manufacturer's protocol. Library preparation was performed using the SMARTer Ultra-Low RNA Kit (Clontech, CA, USA), and cDNA was amplified according to the manufacturer's protocol. Sequencing was

conducted using a next-generation sequencer, an Illumina NovaSeq 6000 platform in 101-base single-end mode. Sequence reads were mapped to mouse reference genome sequences (mm10) using TopHat software (v 2.0.13) combined with Bowtie2 (v 2.2.3) and SAM tools (v 0.1.19). The FPKM values were calculated using Cufflinks software (v 2.2.1). Gene ontology enrichment analysis was performed using DAVID functional annotation bioinformatics microarray analysis (https://david.ncifcrf.gov) and ranked GSEA (v 4.1.0) (http://www.gsea-msigdb.org/gsea/index.jsp).

Stereotaxic injection of G51D α-synuclein into the SNc of mice

Generation and intranigral injection of pre-formed G51D α-synuclein fibrils were performed as described previously[19]. Adult Ddc-hKO1 male mice at 7–8 weeks old were used for the injection. Mice were anesthetized, and saline or G51D α-synuclein (20 μg at 5 μg/μL) were injected into the SNc using a Hamilton microsyringe (Hamilton Co, NV, USA) under stereotaxic surgery (1.3 mm lateral, -2.8 mm posterior from the bregma, 4.3 mm below the dural surface). Unilateral injections were performed for immunohistochemistry, and bilateral injections were performed for RNA-seq analysis.

Immunohistochemistry

At 7 or 12 weeks post-injection, α-synuclein-inoculated mice were deeply anesthetized and perfused transcardially with 4% PFA/PBS. Dissected brains were post-fixed overnight in 4% PFA/PBS and then immersed in PBS containing 30% sucrose solution (30% sucrose/PBS) until sinking as reported previously[55]. Immunohistochemistry was performed on 20 μm serial section cut with a cryostat (Leica Microsystems, Wetzlar, Germany). The primary antibodies used were as follows: mouse anti-phosphorylated-α-synuclein (Ser-129, 1:10,000; Wako, Osaka, Japan), rabbit anti-TH (1:1,000; Calbiochem, CA, USA), and mouse-anti-fatty acid-binding protein 1 (FABP1) (1:200, Abcam, UK). For double immunofluorescence staining, appropriate fluorescent secondary antibodies conjugated to Cy3 and FITC (1:500; Jackson ImmunoResearch) were used. Incubation was performed in PBS for 1 h at room temperature. Sections were washed with PBS three times, counterstained with 4',6-diamidino-2-phenylindole mounting medium (Vectashield, Vector Laboratories), and observed using BZ-9000 (Keyence, Osaka, Japan). For histological analysis, coronal sections were incubated with a biotinylated secondary antibody (1:500; Vector Laboratories), and the reaction products were visualized with avidin-biotin-peroxidase complex (Vector Laboratories) using 3'-diaminobenzidine (Sigma-Aldrich, Missouri, USA) as a chromogen. For the stereological assessment of the total number of TH-positive neurons, serial sections were prepared as reported previously[55]. Every fourth section was stained through the entire extent of the SNc. Cells were counted based on the method described by Furuya et al.[55]. For the assessment of FABP1, three sections from each mouse were analyzed, and the average percentage of FABP1- and Ddc-hKO1-double positive cells was calculated.

Declarations

Acknowledgements

We thank Dr. Bong Gu Kang from John Hopkins University for his technical advice on optimizing the neural dissociation protocol for FACS, and Dr. Cesar Aguirre for providing pre-formed G51D a-synuclein fibrils. We acknowledged the NGS core facility of the Genome Information Research Center at the Research Institute for Microbial Diseases of Osaka University for the support in RNA sequencing. This study was supported by the Takeda Science Foundation and JSPS KAKENHI Grant Numbers 19H05754 and 19K06676.

Author information

These authors contributed equally: Kit-Yeng Sheng, Hideki Hayakawa.

Contributions

KS, SY, HH, YK, and KB conceived, designed, and coordinated the study. KS and HH conducted the experiments. SY, KB, TN, and HM supervised part of the experiments. All authors contributed to the interpretations and conclusions of the study. KS and SY wrote the manuscript.

Competing interests

The author(s) declare no competing interests.

References

1. Klein, M. O. *et al.* Dopamine: Functions, Signaling, and Association with Neurological Diseases. *Cellular and Molecular Neurobiology* **39**, 31–59 (2019).
2. Yasuda, T., Nakata, Y. & Mochizuki, H. α-Synuclein and neuronal cell death. *Molecular neurobiology* **47**, 466–483 (2013).
3. Carrarini, C. *et al.* A stage-based approach to therapy in parkinson's disease. *Biomolecules* **9**, (2019).
4. Bridi, J. C. & Hirth, F. Mechanisms of α-Synuclein induced synaptopathy in parkinson's disease. *Frontiers in Neuroscience* **12**, 1–18 (2018).
5. Maiti, P., Manna, J., Dunbar, G. L., Maiti, P. & Dunbar, G. L. Current understanding of the molecular mechanisms in Parkinson's disease: Targets for potential treatments. *Translational Neurodegeneration* **6**, 1–35 (2017).
6. Schapira, A. H. V., Chaudhuri, K. R. & Jenner, P. Non-motor features of Parkinson disease. *Nature Reviews Neuroscience* **18**, 435–450 (2017).
7. Nakata, Y. *et al.* Accumulation of α-synuclein triggered by presynaptic dysfunction. *Journal of Neuroscience* **32**, 17186–17196 (2012).
8. Araki, K. *et al.* Parkinson's disease is a type of amyloidosis featuring accumulation of amyloid fibrils of α-synuclein. *Proceedings of the National Academy of Sciences of the United States of America* **116**, 17963–17969 (2019).

9. Araki, K. *et al.* Synchrotron FTIR micro-spectroscopy for structural analysis of Lewy bodies in the brain of Parkinson's disease patients. *Scientific Reports* **5**, 1–8 (2015).
10. Mahul-Mellier, A. L. *et al.* The process of Lewy body formation, rather than simply α-synuclein fibrillization, is one of the major drivers of neurodegeneration. *Proceedings of the National Academy of Sciences of the United States of America* **117**, 4971–4982 (2020).
11. Shahmoradian, S. H. *et al.* Lewy pathology in Parkinson's disease consists of crowded organelles and lipid membranes. *Nature Neuroscience* **22**, 1099–1109 (2019).
12. Ikenaka, K., Suzuki, M., Mochizuki, H. & Nagai, Y. Lipids as trans-acting effectors for α-synuclein in the pathogenesis of Parkinson's disease. *Frontiers in Neuroscience* **13**, 1–9 (2019).
13. Guo, J. T. *et al.* Inhibition of vesicular monoamine transporter-2 activity in α-synuclein stably transfected SH-SY5Y cells. *Cellular and Molecular Neurobiology* **28**, 35–47 (2008).
14. Perez, R. G. *et al.* A role for α-synuclein in the regulation of dopamine biosynthesis. *Journal of Neuroscience* **22**, 3090–3099 (2002).
15. Kramer, M. L. & Schulz-Schaeffer, W. J. Presynaptic α-synuclein aggregates, not Lewy bodies, cause neurodegeneration in dementia with lewy bodies. *Journal of Neuroscience* **27**, 1405–1410 (2007).
16. Volpicelli-Daley, L. A. *et al.* Formation of α-synuclein lewy neurite-like aggregates in axons impedes the transport of distinct endosomes. *Molecular Biology of the Cell* **25**, 4010–4023 (2014).
17. Duffy, M. F. *et al.* Lewy body-like alpha-synuclein inclusions trigger reactive microgliosis prior to nigral degeneration. *Journal of Neuroinflammation* **15**, 129 (2018).
18. Du, T., Wu, Z., Luo, H., Lu, S. & Ma, K. Injection of α-syn-98 Aggregates Into the Brain Triggers α-Synuclein Pathology and an Inflammatory Response. *Frontiers in Molecular Neuroscience* **12**, 1–12 (2019).
19. Hayakawa, H. *et al.* Structurally distinct α-synuclein fibrils induce robust parkinsonian pathology. *Movement Disorders* **35**, 256–267 (2020).
20. Luk, K. C. *et al.* Intracerebral inoculation of pathological α-synuclein initiates a rapidly progressive neurodegenerative α-synucleinopathy in mice. *Journal of Experimental Medicine* **209**, 975–988 (2012).
21. Paumier, K. L. *et al.* Intrastriatal injection of pre-formed mouse alpha-synuclein fibrils into rats triggers alpha-synuclein pathology and bilateral nigrostriatal degeneration. *Neurobiology of Disease* **82**, 185–199 (2015).
22. Ekmark-Lewén, S. *et al.* Early fine motor impairment and behavioral dysfunction in (Thy-1)-h[A30P] alpha-synuclein mice. *Brain and Behavior* **8**, 1–14 (2018).
23. Tiklová, K. *et al.* Single-cell RNA sequencing reveals midbrain dopamine neuron diversity emerging during mouse brain development. *Nature Communications* **10**, 1–12 (2019).
24. Hook, P. W. *et al.* Single-Cell RNA-Seq of Mouse Dopaminergic Neurons Informs Candidate Gene Selection for Sporadic Parkinson Disease. *American Journal of Human Genetics* **102**, 427–446 (2018).

25. Tuesta, L. M. *et al.* In vivo nuclear capture and molecular profiling identifies Gmeb1 as a transcriptional regulator essential for dopamine neuron function. *Nature Communications* **10**, 1–12 (2019).
26. Poulin, J. F. *et al.* Defining midbrain dopaminergic neuron diversity by single-cell gene expression profiling. *Cell Reports* **9**, 930–943 (2014).
27. Falkenburger, B. H., Saridaki, T. & Dinter, E. Cellular models for Parkinson's disease. *Journal of Neurochemistry* **139**, 121–130 (2016).
28. Delenclos, M. *et al.* Cellular models of alpha-synuclein toxicity and aggregation. *Journal of Neurochemistry* **150**, 566–576 (2019).
29. Navailles, S. & de Deurwaerdère, P. Contribution of serotonergic transmission to the motor and cognitive effects of high-frequency stimulation of the subthalamic nucleus or levodopa in Parkinson's disease. *Molecular Neurobiology* **45**, 173–185 (2012).
30. Weihe, E., Depboylu, C., Schütz, B., Schäfer, M. K.-H. & Eiden, L. E. Three Types of Tyrosine Hydroxylase-Positive CNS Neurons Distinguished by Dopa Decarboxylase and VMAT2 Co-Expression Eberhard. *Cell Molecular Neurobiology* **26**, 659–678 (2006).
31. Menheniott, T. R. *et al.* Genomic Imprinting of Dopa decarboxylase in Heart and Reciprocal Allelic Expression with Neighboring Grb10. *Molecular and Cellular Biology* **28**, 386–396 (2008).
32. Lein, E. S. *et al.* Genome-wide atlas of gene expression in the adult mouse brain. *Nature* **445**, 168–176 (2007).
33. Saxena, A. *et al.* Trehalose-enhance isolation of neuronal sub-types from adult mouse brain. *Biotechniques* **52**, 381–385 (2012).
34. Su, A. I. *et al.* Large-scale analysis of the human and mouse transcriptomes. *Proceedings of the National Academy of Sciences of the United States of America* **99**, 4465–4470 (2002).
35. Shioda, N. *et al.* FABP3 protein promotes α-synuclein oligomerization associated with 1-Methyl-1,2,3,6-tetrahydropiridine-induced neurotoxicity. *Journal of Biological Chemistry* **289**, 18957–18965 (2014).
36. Cheng, A., Shinoda, Y., Yamamoto, T., Miyachi, H. & Fukunaga, K. Development of FABP3 ligands that inhibit arachidonic acid-induced α-synuclein oligomerization. *Brain Research* **1707**, 190–197 (2019).
37. Sawamoto, K. *et al.* Visualization, direct isolation, and transplantation of midbrain dopaminergic neurons. *Proceedings of the National Academy of Sciences of the United States of America* **98**, 6423–6428 (2001).
38. Matsushita, N. *et al.* Dynamics of tyrosine hydroxylase promoter activity during midbrain dopaminergic neuron development. *Journal of Neurochemistry* **82**, 295–304 (2002).
39. Fernandes, H. J. R. *et al.* Single-Cell Transcriptomics of Parkinson's Disease Human In Vitro Models Reveals Dopamine Neuron-Specific Stress Responses. *Cell Reports* **33**, 108263 (2020).
40. Alza, N. P., Iglesias González, P. A., Conde, M. A., Uranga, R. M. & Salvador, G. A. Lipids at the crossroad of α-synuclein function and dysfunction: Biological and pathological implications.

Frontiers in Cellular Neuroscience **13**, 1–17 (2019).

41. Hozumi, Y., Watanabe, M., Otani, K. & Goto, K. Diacylglycerol kinase β promotes dendritic outgrowth and spine maturation in developing hippocampal neurons. *BMC Neuroscience* **10**, 99 (2009).
42. Kang, Y. *et al.* Sengers Syndrome-Associated Mitochondrial Acylglycerol Kinase Is a Subunit of the Human TIM22 Protein Import Complex. *Molecular Cell* **67**, 457-470.e5 (2017).
43. Tricarico, P. M. *et al.* Mevalonate kinase deficiency and neuroinflammation: Balance between apoptosis and pyroptosis. *International Journal of Molecular Sciences* **14**, 23274–23288 (2013).
44. Sado, M. *et al.* Protective effect against Parkinson's disease-related insults through the activation of XBP1. *Brain Research* **1257**, 16–24 (2009).
45. Yan, C. *et al.* IRE1 promotes neurodegeneration through autophagy-dependent neuron death in the Drosophila model of Parkinson's disease. *Cell Death and Disease* **10**, (2019).
46. Cox, D., Carver, J. A. & Ecroyd, H. Preventing α-synuclein aggregation: The role of the small heat-shock molecular chaperone proteins. *Biochimica et Biophysica Acta - Molecular Basis of Disease* **1842**, 1830–1843 (2014).
47. Ghosh, J. G., Houck, S. A. & Clark, J. I. Interactive sequences in the molecular chaperone, human αB crystallin modulate the fibrillation of amyloidogenic proteins. *International Journal of Biochemistry and Cell Biology* **40**, 954–967 (2008).
48. Babak, T. *et al.* Genetic conflict reflected in tissue-specific maps of genomic imprinting in human and mouse. *Nature Genetics* **47**, 544–549 (2015).
49. Gregg, C. *et al.* High-resolution analysis of parent-of-origin allelic expression in the mouse brain. *Science* **329**, 643–648 (2010).
50. George, S. H. L. *et al.* Developmental and adult phenotyping directly from mutant embryonic stem cells. *Proceedings of the National Academy of Sciences of the United States of America* **104**, 4455–4460 (2007).
51. Pucéat, M. Protocols for cardiac differentiation of embryonic stem cells. *Methods* **45**, 168–171 (2008).
52. Susaki, E. A. *et al.* Whole-brain imaging with single-cell resolution using chemical cocktails and computational analysis. *Cell* **157**, 726–739 (2014).
53. Fischer, J. *et al.* Prospective isolation of adult neural stem cells from the mouse subependymal zone. *Nature Protocols* **6**, 1981–1989 (2011).
54. Walker, T. L. & Kempermann, G. One mouse, two cultures: Isolation and culture of adult neural stem cells from the two neurogenic zones of individual mice. *Journal of Visualized Experiments* 1–9 (2014) doi:10.3791/51225.
55. Furuya, T. *et al.* Caspase-11 Mediates Inflammatory Dopaminergic Cell Death in the 1-Methyl-4-Phenyl-1,2,3,6-Tetrahydropyridine Mouse Model of Parkinson's Disease. *Journal of Neuroscience* **24**, 1865–1872 (2004).

Figures

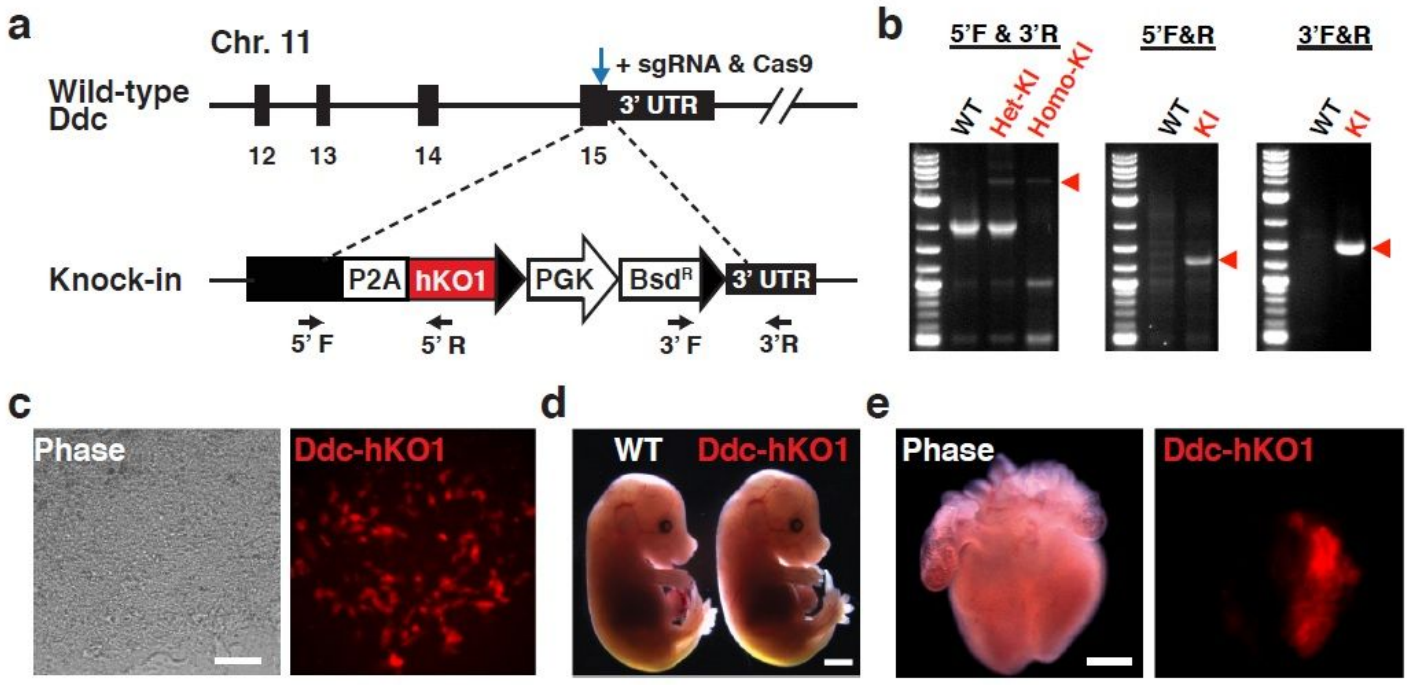

Figure 1

Establishment of Ddc-hKO1 knock-in reporter mice. (a) Schematic representation of Ddc-hKO1 knock-in strategy at dopa-decarboxylase (Ddc) locus. Arrows indicate the PCR primer sets for the genotyping of the knock-in site. Blue arrow indicates the targeted site of sgRNA. (b) Representative results of PCR-based genotyping of wild type, and Ddc-hKO1 knock-in embryonic stem cells (ESCs). The positions of the primers were indicated in (a). WT, wild type; Het-KI, heterozygous Ddc-hKO1; Homo-KI, homozygous Ddc-hKO1. Red arrowheads indicate the expected size of amplicon containing knock-in cassette. (c) Representative images of cardiac cell lineages differentiated from the knock-in ESCs. Scale bar, 50 mm. (d) Representative images of E18.5 embryos of WT and Ddc-hKO1 mice. Scale bar, 2 mm. (e) Representative images of E15.5 embryonic heart of Ddc-hKO1 mouse. Scale bar, 500 mm.

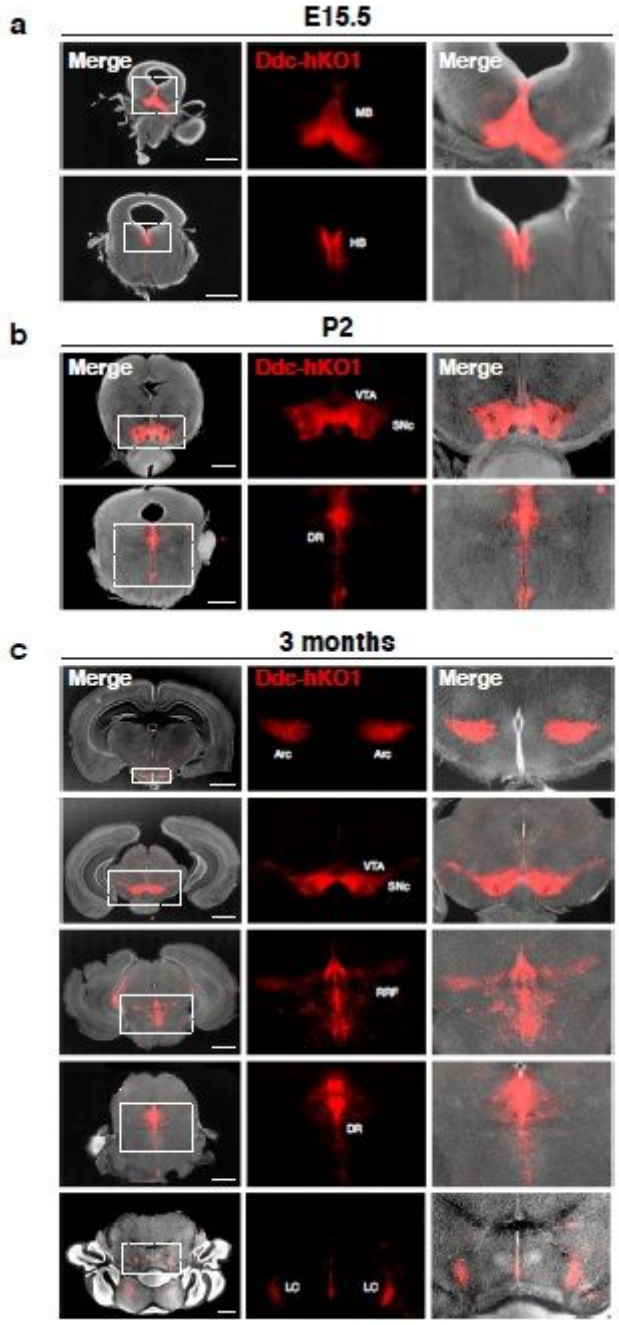

Figure 2

Expression pattern of Ddc-hKO1 in embryonic, neonatal, and adult mouse brains. (a-c) Representative images of vibratome sections of the whole brain in the coronal plane at E15.5 (a), P2 (b), and 3 months old (c). Thickness, 200 mm. Scale bar, 200 mm. MB, midbrain; HB, hindbrain; VTA, ventral tegmental area; SNc, substantia nigra pars compacta; DR, dorsal raphe nucleus; Arc, arcuate nucleus; RRF, retrorubral field; LC, locus coerules.

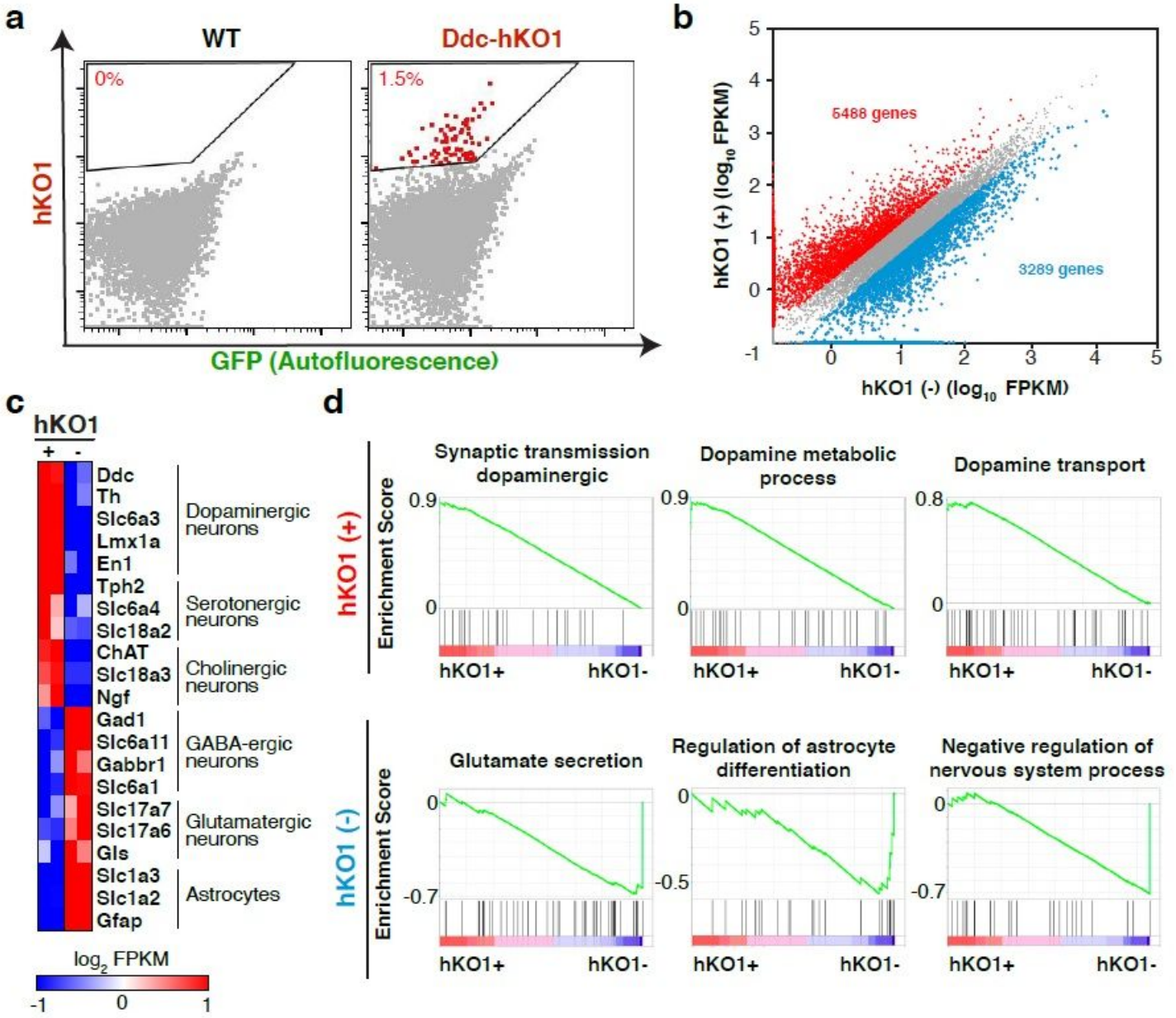

Figure 3

Purification of dopaminergic neurons from Ddc-hKO1 mouse. (a) Representative FACS dot plots showing the gating strategy for the recovery of hKO1-positive neurons from Arc, VTA, SNc, DR, RRF, and LC of WT and Ddc-hKO1 mouse brains. Red dots represent the hKO1-positive neurons. (b) Scatter plot of RNA-Seq gene expression data comparing hKO1-positive and hKO1-negative populations. Fold change (FC) > 2. Red dots indicate genes highly expressed in hKO1-positive neurons, and blue dots indicate genes highly expressed in hKO1-negative neurons. (c) Heat map representation of expression levels of selected neuronal and non-neuronal marker genes. (d) Representative gene set enrichment analysis (GSEA) results enriched in hKO1-positive and hKO1-negative populations. VTA, ventral tegmental area; SNc, substantia nigra pars compacta; DR, dorsal raphe nucleus; Arc, arcuate nucleus; RRF, retrorubral field; LC, locus coerules; WT, wild type.

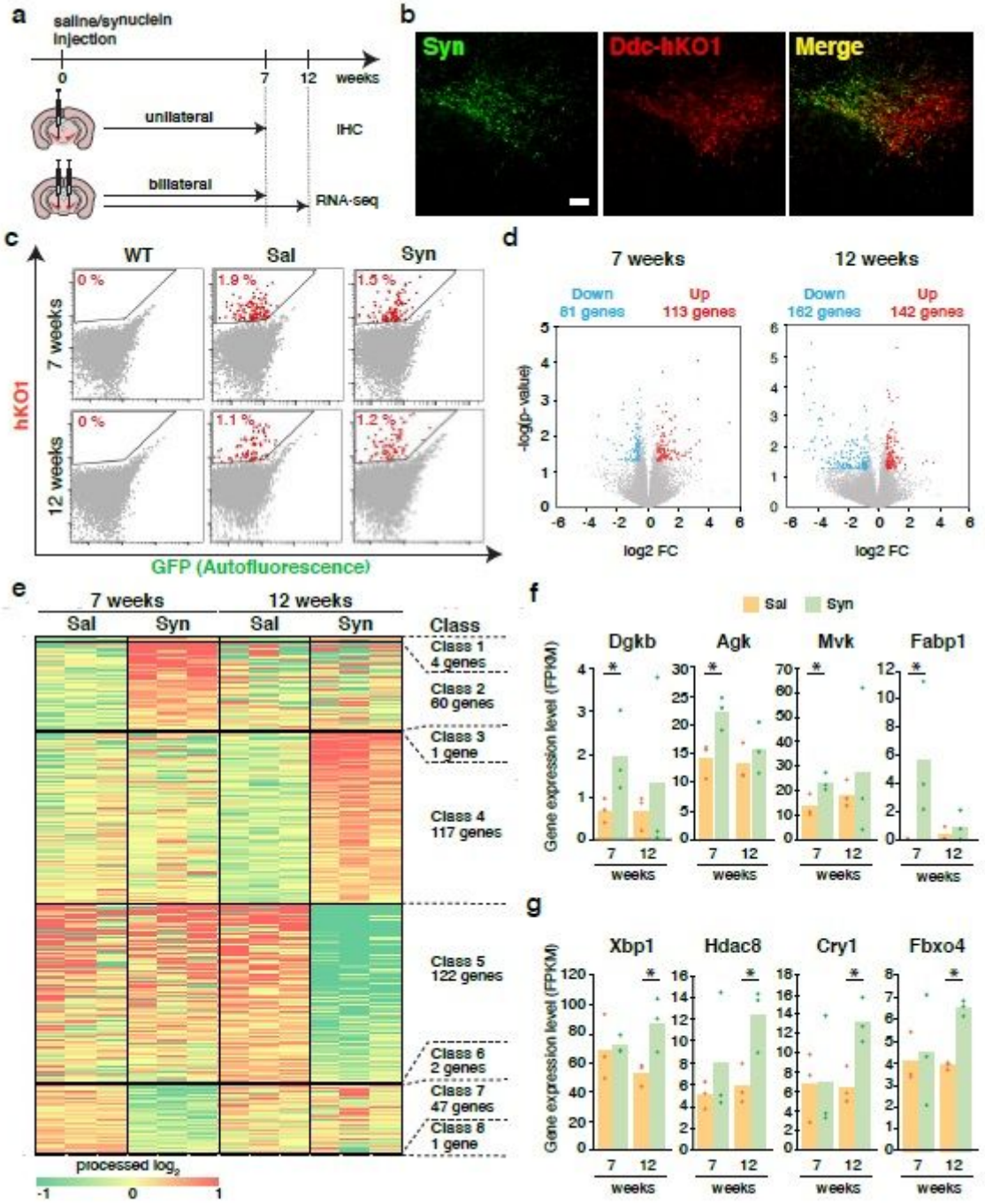

Figure 4

Transcriptome profiling of a-synuclein accumulated neuron using Ddc-hKO1 mice. (a) Experimental scheme of transcriptome analysis of purified dopaminergic neurons from a-synuclein-injected brain. a-synuclein or saline was injected into the SNc of Ddc-hKO1 mouse brain unilaterally or bilaterally, and harvested at 7 weeks for immunohistochemistry and 7 or 12 weeks for RNA-seq analysis. (b) Representative images of immunohistochemistry of accumulated a-synuclein in the Ddc-hKO1 brain at 7 weeks. Scale bar, 100 mm. (c) Representative FACS dot plots showing the gating strategy for collecting survived hKO1-positive neurons from the injected brains. Red dots indicate hKO1-positive neurons. (d)

Volcano plot showing the differentially expressed genes (DEGs) in hKO1-positive neurons between synuclein- and saline-injected mice. Upregulated and downregulated genes were highlighted by red and blue dots (FC > 1.5, FPKM > 1, p < 0.05) n = 3. (e) Heat map representation showing the classification of DEGs and gene numbers in each class. (f, g) Examples of DEGs in hKO1-positive neurons of a-synuclein-injected mice at 7 weeks (f) and 12 weeks (g). FACS, fluorescence-activated cell sorter; Sal, saline-injected; Syn, a-synuclein-injected brains. *P < 0.05, t-test, n = 3.

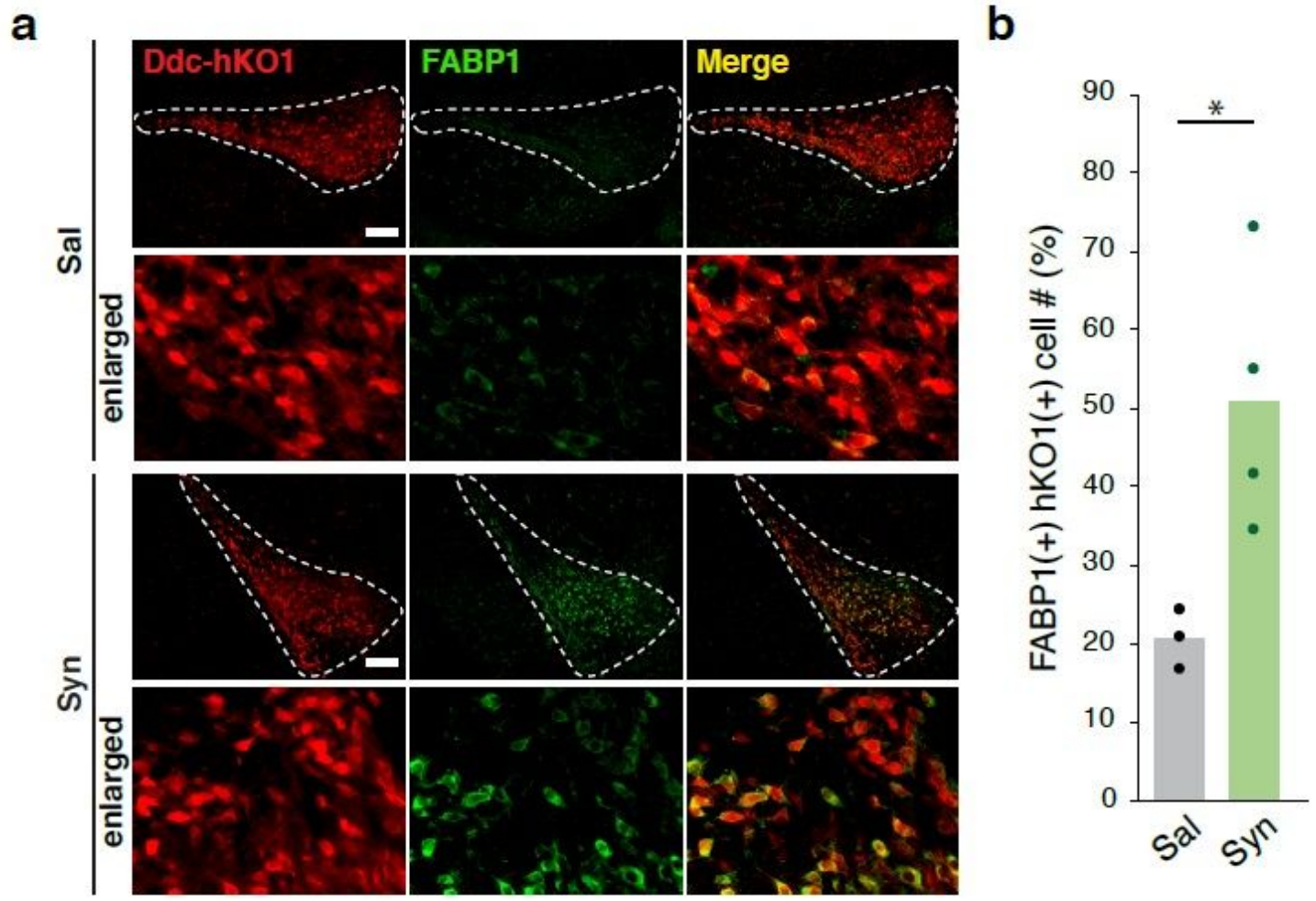

Figure 5

FABP1 activation in the dopaminergic neurons during a-synuclein accumulation. (a) Representative immunostaining images showing the FABP1 expression in the VTA and SNc of injected mouse brains at 7 weeks. Scale bar: 100 mm. Dotted line indicates the VTA and SNc. (b) Bar graph showing the ratio of FABP1-positive cells in hKO1-positive cells at the VTA and SNc regions of saline- or a-synuclein-injected mouse brains at 7 weeks. Each dot represents the actual value obtained from the individual mouse. FACS, fluorescence-activated cell sorter; VTA, ventral tegmental area; SNc, substantia nigra pars compacta; Sal, saline-injected; Syn, a-synuclein-injected. *P < 0.05, t-test, Sal: n = 3, Syn: n = 4.

Supplementary Files

This is a list of supplementary files associated with this preprint. Click to download.

- SupplementaryFigures.pdf
- SupplementaryTables.pdf